Pulse-based variational quantum optimization and metalearning in superconducting circuits

Yapeng Wang,[1] Yongcheng Ding,[1,2,*] Francisco Andrés Cárdenas-López,[3,†] and Xi Chen[4,‡]

[1] *Institute for Quantum Science and Technology, Department of Physics, Shanghai University, Shanghai 200444, China*

[2] *Department of Physical Chemistry, University of the Basque Country UPV/EHU, Apartado 644, 48080 Bilbao, Spain*

[3] *Peter Grünberg Institute, Forschungszentrum Jülich, Institute of Quantum Control (PGI-8), D-52425 Jülich, Germany*

[4] *Instituto de Ciencia de Materiales de Madrid (CSIC), Cantoblanco, E-28049 Madrid, Spain*

(Received 7 May 2024; revised 29 June 2024; accepted 17 July 2024; published 5 August 2024)

Solving optimization problems using variational algorithms stands out as a crucial application for noisy intermediate-scale devices. Instead of constructing gate-based quantum computers, our focus centers on designing variational quantum algorithms within the analog paradigm. This involves optimizing parameters that directly control pulses, driving quantum states toward target states without the necessity to compile a quantum circuit. In this work, we introduce pulse-based variational quantum optimization (PBVQO) as a hardware-level framework. We illustrate the framework by optimizing external fluxes on superconducting quantum interference devices, effectively driving the wave function of this specific quantum architecture to the ground state of an encoded problem Hamiltonian. Given that the performance of variational algorithms relies heavily on appropriate initial parameters, we introduce a global optimizer as a metalearning technique to tackle a simple problem. The synergy between PBVQO and metalearning provides an advantage over conventional gate-based variational algorithms.

DOI: 10.1103/PhysRevApplied.22.024009

I. INTRODUCTION

Quantum computing has emerged as a promising field with the potential to revolutionize computational methodologies. Unique properties such as superposition and quantum entanglement in quantum mechanics offer theoretical speedups by embedding problems into quantum systems. With advancements in experimental techniques, we now find ourselves in the noisy intermediate-scale quantum (NISQ) era, where quantum computers demonstrate capabilities for solving complex problems [1]. Among the most intriguing applications of quantum computing in this era is quantum optimization [2]. Broadly, quantum optimization entails utilizing quantum devices to determine the ground state of a Hamiltonian that encodes a classical cost function. It finds its roots in the adiabatic theorem, wherein a system is prepared in the ground state of a simple Hamiltonian and evolved to the problem Hamiltonian, guaranteeing convergence to the problem's ground state if adiabatic criteria are met. This concept gave rise to quantum annealing and the development of quantum annealers within the analog quantum computing paradigm [3–5], obviating the need for constructing quantum gates. Subsequently, it inspired the quantum approximate optimization algorithm (QAOA) [6,7] as one of the most renowned variational quantum algorithms (VQAs) [8,9]. Through incooperation with classical optimizers, gate parameters within the quantum circuit are iteratively optimized to minimize a cost function, typically the energy expectation of a Hamiltonian. This showcases the utility of state-of-the-art quantum devices across interdisciplinary fields [10–13].

Various approaches have been proposed to enhance the performance of QAOA. It operates as a bang-bang control, alternating between evolving the mixing and problem Hamiltonians [14]. Optimal control theory enables analytical solutions for optimal procedures within bounded operating times, featuring square-pulse-based QAOA on two sides and smooth annealing in between [15]. This resembles mimicking QAOA in the digital-analog quantum computing paradigm [16,17], where quantum gates and specific Hamiltonian evolutions coexist. Another perspective focuses on the circuit level, akin to quantum machine learning [18], proposing different structures as

*Contact author: jonzen.ding@gmail.com
†Contact author: f.cardeans.lopez@fz-juelich.de
‡Contact author: xi.chen@csic.es

ansatz to enhance model performance. For instance, the quantum alternating operator ansatz replaces trivial transverse local operators with entangling operators tailored to specific problems [19]. In addition, adaptive QAOA dynamically selects the mixer from a preselected operator pool [20]. Moreover, shortcuts-to-adiabaticity has been introduced from quantum control to quantum computing [21], as parameter searching in QAOA is equivalent to optimizing a discretized annealing schedule. Approximate counterdiabatic terms can be easily implemented in quantum circuits to suppress energy excitation, thereby enhancing the performance of variational quantum optimization [22–24]. These recently proposed QAOA variants, combined with classical optimizers, have been benchmarked up to 28 qubits [25].

Here, we aim to introduce an alternative approach to variational quantum optimization by concentrating on optimizing parameters that characterize control pulses. The advantages of pulse-based methods over traditional gate-based approaches are becoming increasingly evident. Pulse-based optimization offers faster state preparation, simpler implementation, and greater freedom in navigating the quantum state space. Recently, pulse-based models have been proposed to enhance VQAs, such as extending variational quantum eigensolver (VQE) to Ctrl-VQE [26,27], modifying ansatz to PANSATZ [28], and exploring applications in quantum machine learning [29]. Previous related work in quantum optimization has explored analog versions of QAOA and realized variational coherent annealing by introducing auxiliary terms [30,31]. In addition, a comparison between gate-model and pulse-based models has been conducted on bipotent quantum architectures where quantum gates are not readily available for arbitrary qubits [32]. Building upon these previous results, we propose pulse-based variational quantum optimization (PBVQO), with the objective of solving quantum optimization problems at the level of control pulses on realistic quantum devices. Furthermore, we recognize that local optimization of VQAs can be computationally expensive, requiring additional circuit depth and numerous measurements. By initializing parameters close to global minima, the number of optimization iterations can be reduced significantly. This observation motivates the exploration of metalearning techniques, whose feasibility has been demonstrated in gate-model QAOA with counterdiabaticity [33].

The remainder of the paper is organized as follows. In Sec. II, we introduce the concept of PBVQO, which is a hardware-agnostic framework requiring single-qubit operations and tunable two-body interactions. Then we test our method by combining it with a digital-analog superconducting circuit architecture in Sec. III. In Sec. IV, we demonstrate our protocol through numerical experiments aimed at solving the MAX-CUT problem with up to 8 qubits. To tackle optimization challenges, we utilize a combination of BFGS, a quasi-Newtonian optimizer for parameter updates, and genetic algorithms to preselect suitable parameter initializations. In addition, in Sec. V, we present a comparative analysis with conventional gate-based QAOA to highlight the advantages of our approach. Finally, the conclusion and outlook are presented in Sec. VI.

II. PULSE-BASED OPTIMIZATION

We exemplify PBVQO by solving the MAX-CUT problem. At the hardware level, we assume that the hardware architecture can only directly realize two-body neighboring interaction as an Ising spin chain or an Ising spin ring by connecting the first and last qubit with periodic boundary conditions. To avoid searching for composite pulses to implement effective many-body interactions, we utilize the architecture to solve 2-regular graphs without any disconnected cycles, meaning the degree of each node is 2, which can be easily embedded into the architecture by topology. Thus, the problem is equivalent to finding the ground state of an antiferromagnetic Ising ring. We assume that the effective hardware Hamiltonian includes only local spin operator and neighboring interaction, which can be expressed as

$$H_{\mathrm{PBVQO}} = \sum_j \frac{\omega_j}{2}\sigma_j^z + P(t)\sigma_j^y\sigma_{j+1}^y, \tag{1}$$

where $P(t)$ is the pulse to be optimized, and $\sigma_j^y\sigma_{j+1}^y$ can be replaced by other interaction terms depending on the capabilities of the platform. This effective Hamiltonian is feasible in various quantum devices without loss of generality. In principle, the pulse ansatz $P(t)$ can be of any form, as long as it can be implemented on the specific quantum device. However, in practical implementation, not all pulses are realizable, so a filter $F[P(t)]$ is required for pulse. For simplicity, we illustrate the PBVQO framework by assuming that the optimal pulse can be expressed as a series of trigonometric functions

$$P(t) = \sum_{i=1}^{n} A_i \sin\left[(2i-1)\pi t + \phi_i\right], \tag{2}$$

where A_i are the pulse amplitudes, $t \in [0, T]$ is the operation time, and ϕ_i are the phases. The trigonometric functions resemble the annealing schedule used in variational quantum annealing [34], though the mechanism is not exactly the same. In this context, the series allows for the expression of an arbitrary function by providing sufficient freedom with amplitudes and phases.

In contrast, the conventional QAOA for MAX-CUT problems prepares the system in the product state $|+\rangle^{\otimes N}$, which is an eigenstate of the mixing Hamiltonian (mixer) $H_{\mathrm{mix}} = \sum_j \sigma_j^x$, and then let the system evolve by

alternate application of the problem Hamiltonian $H_p = \sum_{\langle i,j\rangle\in\mathcal{G}} \sigma_i^z\sigma_j^z$ ($\mathcal{G}$ is the graph to be solved) with the mixing ones for p rounds. In other words, we compute the evolution of the system through the product $|\Psi_f\rangle = \prod_j^p \exp(-i\beta_j H_{\text{mix}}) \exp(-i\gamma_j H_p)|+\rangle^{\otimes N}$. QAOA aims for finding the set of parameters $\{\beta_j, \gamma_j\}$ that minimize the averaged energy of the problem Hamiltonian, $\langle\Psi_f|H_p|\Psi_f\rangle$ so that $|\Psi_f\rangle$ is the ground state of the problem Hamiltonian. Measuring the Z-Pauli strings of the problem, we obtain the MAX-CUT of the graph, if the optimization procedure was successful. From the annealing perspective, finding the parameters $\{\beta_j, \gamma_j\}$ is equivalent to find the optimal schedule function for a digitalized quantum annealing process

$$H_{\text{QA}} = B(t)\sum_j \sigma_j^x + \Gamma(t)\sum_{\langle i,j\rangle\in\mathcal{G}} \sigma_i^z\sigma_j^z, \tag{3}$$

where $\beta_i^* = B(i\delta t)\delta t$ and $\gamma_i^* = \Gamma(i\delta t)\delta t$ are the optimal parameters describing the schedule.

We realize that in PBVQO, it is not necessary to prepare the system in the state $|+\rangle^{\otimes N}$. Instead, it is more advantageous to start in the state $|0\rangle^{\otimes N}$, which is an eigenstate of the mixing Hamiltonian in our architecture, $\sum_j (\omega_j/2)\sigma_j^z$. Unlike the typical QAOA realization, we do not switch off the mixing Hamiltonian. Moreover, we will consider the two-body interactions to be $\sum_{\langle i,j\rangle} \sigma_i^y\sigma_j^y$, which remain always turned-on. Consequently, we need to engineer the pulse sequences such that both Hamiltonian encodes the ground state of the MAX-CUT Hamiltonian $\tilde{H}_p = \sum_{\langle i,j\rangle\in\mathcal{G}} \sigma_i^x\sigma_j^x$.

The workflow of PBVQO consists of the following steps. We initialize the pulse ansatz by randomly selecting both amplitudes and phases. Then, the pulse is filtered to obtain $F[P(t)]$. Next we calculate the dynamics of the mixing and problem Hamiltonian, resulting in the state $|\Psi_f\rangle$. Afterward, we compute the average of the energy $\langle\Psi_f|\tilde{H}_p|\Psi_f\rangle$ and we update the parameters $\{A_i, \phi_i\}$ using a classical optimizer, such as BFGS. When the optimization converges according to our hyperparameters, we measure the system on the x-axis, obtaining the classical configuration of the MAX-CUT problem. We evaluate the PBVQO performance by computing the error rate R, defined as

$$R = \left|\frac{\langle\Psi_f^*|\tilde{H}_p|\Psi_f^*\rangle - E_g}{E_g}\right|, \tag{4}$$

where E_g is the ground energy of $\tilde{H}_p$ obtained by numerically diagonalizing the Hamiltonian.

III. HARDWARE ARCHITECTURE

We hereby introduce the superconducting circuit architecture employed for variational quantum optimization,

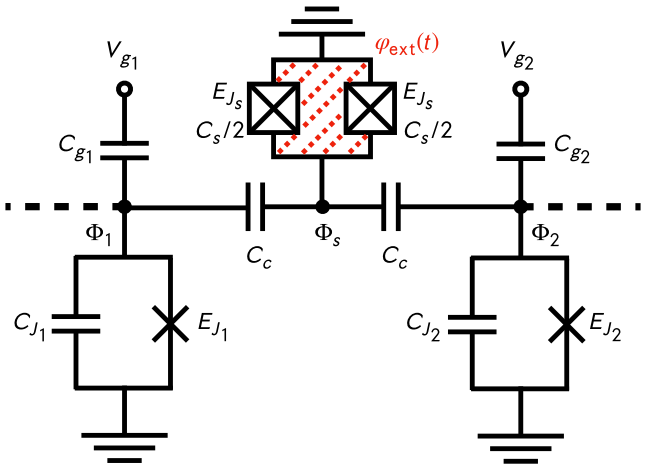

FIG. 1. Schematic circuit representation of the model implementing the PBVQO. Two charge qubits are coupled through a grounded SQUID. The only tunable parameter is the external flux φ_{ext} through the SQUID, indicated by the red shaded region.

which was originally proposed for digital-analog quantum simulation [35]. The minimal structure consists of two charge qubits and a grounded superconducting quantum interference device (SQUID) as a coupler. Each charge qubit consists of a capacitance $C_{J\ell}$ parallel connected to a Josephson junction with energy $E_{J\ell}$ and biased with an external voltage source $V_{g\ell}$ as depicted in Fig. 1. Moreover, the SQUID is formed by a closed loop embedded with two identical Josephson junctions of capacitances $C_s/2$ and Josephson energies $E_{Js}/2$, respectively. In addition, the loop is threaded by an external magnetic flux $\varphi_{\text{ext}}(t)$. We denote by Φ_1, Φ_2, and Φ_s the fluxes describing the charge qubits and the SQUID, respectively. The circuit Lagrangian reads

$$\mathcal{L} = \sum_{j=1,2,s}\left[\frac{C_{J_j}\dot{\Phi}_j^2}{2} + \frac{C_{g_j}(\dot{\Phi}_j - V_{g_j})^2}{2} + \frac{C_c(\dot{\Phi}_j - \dot{\Phi}_s)^2}{2} + E_{J_j}\cos(\varphi_j)\right] + \frac{C_{J_s}\dot{\Phi}_s^2}{2} + E_{J_s}^{\text{eff}}[\varphi_{\text{ext}}(t)]\cos(\varphi_s), \tag{5}$$

here the overdot notation represents derivation with respect to time. Moreover, $E_{J_s}^{\text{eff}}[\varphi_{\text{ext}}(t)] = 2E_{J_s}|\cos[\varphi_{\text{ext}}(t)]|$ is the tunable Josephson energy of the SQUID with $\varphi_j = \Phi_j/\varphi_0$ being the superconducting phase.

The idea of this architecture is to manipulate the coupling strength between both charge qubit by modulating the external phase $\varphi_{\text{ext}}(t)$ without exciting the SQUID, in this case we need to assume that the latter operates in the so-called *high-plasma frequency* and *low-impedance* approximation [36,37] where it is possible to factorize the SQUID from the system dynamics similar to perturbative diagonalization based on Schrieffer-Wolff transformation [38]. Then for eliminating the SQUID degree of freedom,

we compute the Euler–Lagrange equation of $\mathcal{L}$ obtaining

$$C_{\Sigma_1}\ddot{\Phi}_1 - C_c\ddot{\Phi}_s + \frac{E_{J_1}}{\varphi_0}\sin(\varphi_1) = 0, \tag{6a}$$

$$C_{\Sigma_2}\ddot{\Phi}_2 - C_c\ddot{\Phi}_s + \frac{E_{J_2}}{\varphi_0}\sin(\varphi_2) = 0, \tag{6b}$$

$$C_{\Sigma_s}\ddot{\Phi}_s - C_c(\ddot{\Phi}_1 + \ddot{\Phi}_2) + \frac{E_{J_s}^{\text{eff}}[\varphi_{\text{ext}}(t)]}{\varphi_0}\sin(\varphi_s) = 0. \tag{6c}$$

Here, C_{Σ_j} is the total capacitance of each nodes. The high-plasma frequency allows us to assume that the variation on the fluxes on the charge qubits are larger than in the SQUID, i.e., $\ddot{\Phi}_{1(2)} \gg \ddot{\Phi}_s$; moreover, the low-impedance regime refers to almost no current flows on the SQUID such that we can operate the SQUID in the linearized regime [36]. These conditions permit us to express φ_s in terms of the other node variables:

$$\varphi_s = \sum_j -\frac{C_c E_{J_j}\sin(\varphi_j)}{E_{J_s}^{\text{eff}} C_{\Sigma_j}}. \tag{7}$$

Now, we have to perform the same reasoning to the SQUID charge. To do so, we compute the canonical conjugate momenta $\vec{Q} = \vec{\nabla}_{\dot{\vec{\Phi}}}\mathcal{L}$

$$\vec{Q} = \begin{pmatrix} C_{\Sigma_1}\dot{\Phi}_1 - C_c\dot{\Phi}_s - C_{g_1}V_{g_1} \\ C_{\Sigma_2}\dot{\Phi}_2 - C_c\dot{\Phi}_s - C_{g_2}V_{g_2} \\ C_{\Sigma_s}\dot{\Phi}_s - C_c(\dot{\Phi}_1 + \dot{\Phi}_2) \end{pmatrix}, \tag{8}$$

and apply the high-plasma approximation for eliminating the terms proportional to $\dot{\Phi}_s$, leading to

$$Q_s = -C_c\sum_j \frac{Q_j + C_{g_j}V_{g_j}}{C_{\Sigma_j}}. \tag{9}$$

The conditions in Eq. (7) and in Eq. (9) eliminated the SQUID degree of freedom such that the effective qubit-qubit Hamiltonian can be expressed as

$$H = \sum_{j=1,2}\left[\mathcal{H}_j + \mathcal{H}_{\text{ctrl,j}}\right] + \mathcal{H}_c, \tag{10}$$

where $\mathcal{H}_j$ and are the effective charge qubit and control Hamiltonian, whereas $\mathcal{H}_c$ corresponds to the interaction Hamiltonian given by

$$\mathcal{H}_j = \frac{Q_j^2}{2\tilde{C}_{J_j}} - E_{J_j}\cos\varphi_j + g[\varphi_{\text{ext}}(t)]\sin^2(\varphi_j), \tag{11a}$$

$$\mathcal{H}_{\text{ctrl,j}} = \tilde{n}_{g_j}(t)Q_j, \tag{11b}$$

$$\mathcal{H}_c = g[\varphi_{\text{ext}}(t)]\sin(\varphi_1)\sin(\varphi_2), \tag{11c}$$

where we define the effective capacitances $\tilde{C}_{J_j}$ and $\tilde{C}_{J_s}$ as

$$\tilde{C}_{J_j} = \frac{C_*^3}{C_k(2C_c + C_s) + C_c(C_c + C_s)}, \tag{12}$$

$$\tilde{C}_{J_s} = \frac{C_c C_*^3}{(C_c + C_1)(C_c + C_2)}, \tag{13}$$

where $C_*^3 = C_c(C_1 + C_2)(C_s + C_c) + C_c^2 C_s + C_1 C_2(2C_c + C_s)$ and $C_j = C_{g_j} + C_{J_j}$ ($j \in \{1,2\}$ and k is the other element). The dimensionless gate charges are given by

$$\tilde{n}_{g_j}(t) = -\frac{C_{g_j}}{2e\tilde{C}_{J_j}}V_{g_j} - \frac{\tilde{C}_{J_j}C_c^2 C_{g_k}}{2eC_*^3\tilde{C}_{J_j}}V_{g_k}. \tag{14}$$

Finally, $g[\varphi_{\text{ext}}(t)]$ is the effective coupling strength defined as

$$g[\varphi_{\text{ext}}(t)] = \frac{C_c^2 E_{J_1}E_{J_2}}{E_{J_s}^{\text{eff}}(C_1 + C_c)(C_2 + C_c)}. \tag{15}$$

We quantize the Hamiltonian by promoting quantum operators $\hat{Q}_j = -2e\hat{n}_j$ and $\hat{\varphi}_j$ satisfying canonical commutation relation $[\hat{n}_j, \exp(\pm i\hat{\varphi}_j)] = \exp(\pm i\hat{\varphi}_j)$, substituting Eq. (9) and (7) into the Hamiltonian (10), we obtain for the charge qubit Hamiltonian

$$\mathcal{H}_j = 4E_{Cj}n_j^2 - E_{J_j}\cos\varphi_j + g[\varphi_{\text{ext}}(t)]\sin^2(\varphi_j), \tag{16}$$

where $E_{Cj} = e^2/2\tilde{C}_{J_j}$ is the charge energy. In the charge basis representation, the Hamiltonian in Eq. (10) can be expressed in the two-level approximation as follows

$$H = \sum_{j=1,2}\left[\frac{\omega_j}{2}\sigma_j^z + \Omega_j(t)(n_{0,1}|g\rangle\langle e| + \text{c.c.})\right] + \frac{g[\varphi_{\text{ext}}(t)]}{4}\sigma_1^y\sigma_2^y, \tag{17}$$

where $\omega_j = E_{J_j}$ is the transition frequency of the jth charge qubit. The effective circuit Hamiltonian has three different contributions; the free energy term setting the transition frequency, the single-qubit interaction with drive amplitude $\Omega_j(t)$ and the tunable interaction term, note as the matrix element of the charge operator are real, we can implement an X or Y rotation just by changing the relative phase of the external charge offset $\tilde{n}_{g_j}(t)$. In addition, in this architecture, depending on the scheduling of the external voltages $V_{g_j}(t)$ and the external flux $\varphi_{\text{ext}}(t)$ we are able to dynamically *switch off* the two-qubit interaction while implementing the single-qubit rotations and vice versa, allowing us to implement the digital-analog QAOA dynamics.

On the other hand, the superconducting architecture discussed here is also applicable for implementing gate models by selecting drive frequencies that activate/deactivate certain process in the Hamiltonian in Eq. (17). This can be achieved by assuming that the external flux contains a constant dc and time-varying ac component of the form

$$\varphi_{\rm ext}(t) = \varphi_{\rm dc} + \varphi_{\rm ac}(t), \tag{18}$$

here, we assume that $\varphi_{\rm ac}(t)$ can be decomposed using the pulse defined in Eq. (2):

$$\varphi_{\rm ac}(t) = A_1 \cos(\nu_1 t + \tilde{\phi}_1) + A_2 \cos(\nu_2 t + \tilde{\phi}_2); \tag{19}$$

here, we impose the condition $|A_1|, |A_2| \ll |\varphi_{\rm dc}|$ such that the effective inductance can be expressed as

$$\begin{aligned} \frac{1}{E_{J_s}^{\rm eff}} &\approx \frac{1}{\bar{E}_{J_s}}\left[1 + \frac{\sin(\varphi_{\rm dc})}{\cos(\varphi_{\rm dc})}\varphi_{\rm ac}(t)\right], \\ \bar{E}_{J_s} &= 2E_{J_s}\left|\cos(\varphi_{\rm dc})\right|. \end{aligned} \tag{20}$$

Therefore, we reformulate the Hamiltonian (17) as

$$H = \sum_{j=1,2}\left[\frac{\omega_j}{2}\sigma_j^z + \frac{\Omega_j(t)}{2}\sigma_j^x\right] + \left[g_0 + g_1\varphi_{\rm AC}(t)\right]\sigma_1^y\sigma_2^y, \tag{21}$$

where the always-on and tunable coupling strength reads

$$\begin{aligned} g_0 &= \frac{C_c^2 E_{J_1} E_{J_2}}{4(C_1 + C_c)(C_2 + C_c)\bar{E}_{J_s}}, \\ g_1 &= \frac{C_c^2 E_{J_1} E_{J_2}}{4(C_1 + C_c)(C_2 + C_c)\bar{E}_{J_s}}\frac{\sin(\varphi_{\rm dc})}{\cos(\varphi_{\rm dc})}. \end{aligned} \tag{22}$$

We now proceed by expressing the Hamiltonian in the interaction picture, assuming that there is no drive $\Omega_j(t) = 0$, and performing the rotating wave approximation obtaining the Hamiltonian

$$\hat{\mathcal{H}}_I = \frac{g_1}{4}\left(M_-\sigma_1^x\sigma_2^x + M_+\sigma_1^y\sigma_2^y - N_+\sigma_1^x\sigma_2^y + N_-\sigma_1^y\sigma_2^x\right), \tag{23}$$

where $M_\pm = A_1\cos\tilde{\phi}_1 \pm A_2\cos\tilde{\phi}_2$ and $N_\pm = A_1\sin\tilde{\phi}_1 \pm A_2\sin\tilde{\phi}_2$. This approach allows us to engineer the effective two-body interaction required in the algorithm by the adequate selection of the amplitudes and phases of the external flux $\varphi_{\rm ac}(t)$. For instances, we can engineer the standard QAOA the mixing Hamiltonian XX by setting $\tilde{\phi}_1 = \tilde{\phi}_2 = 0$ and $A_1 = -A_2$ obtaining

$$H_{XX} = \frac{g_1 A_1}{2}\sigma_1^x\sigma_2^x = G\frac{A_1}{2\cos(\varphi_{\rm dc})}\frac{\sin(\varphi_{\rm dc})}{\cos(\varphi_{\rm dc})}\sigma_1^x\sigma_2^x. \tag{24}$$

Thus, this architecture allows us to implement directly the problem-Hamiltonian dynamics $U(-i\beta\sigma_1^x\sigma_2^x)$, making the approach more efficient than compile the problem in terms of single-qubit rotations and entangling CNOT gates. The price to pay is that the condition $|A_1| \ll |\varphi_{\rm dc}|$ bounds our maximal gating time, making the algorithm susceptible to noise and decoherence. A naive approach for accelerating the gating time relies upon setting dc component close to $\varphi_{\rm dc} = \pi/2$. Nevertheless, such approach is not valid because the energy spectrum of the system shrinks, leading to divergencies [39]. Another approach is to use the architecture for engineering the counterdiabatic (CD) Hamiltonian of the QAOA [22,23]: $XY + YX$ for other selection of the pulse parameters. Thus, the scheduling of the whole QAOA may include the pulses for the single-qubit rotations, the action of the entangling gates and the inclusion of the CD evolution.

Note that from the Hamiltonian perspective, we can implement PBVQO by setting $P(t) = g[\varphi_{\rm ext}(t)]/4$. However, the proposed trigonometrical ansatz does not match such coupling because $g[\varphi_{\rm ext}(t)]$ is positive. Moreover, we may encounter errors due to the always-on coupling g_0 during PBVQO. To address these issues, we can filter our pulses considering such experimental constrains under the relation:

$$F[P(t)] = \begin{cases} G, & -G \le P(t) < G, \\ |P(t)|, & \text{otherwise}, \end{cases} \tag{25}$$

where $G = C_c^2 E_{J_1} E_{J_2}/8E_{J_s}(C_1 + C_c)(C_2 + C_c)$ is the bound on the coupling strength.

IV. NUMERICAL EXPERIMENTS

A. Baseline

PBVQO imposes no limit on the operation time; thus, control pulses can be periodic in time, mimicking Floquet engineering protocols. In light of this, our first step is to analyze the role of the pulse duration T in our model's performances, making it a free parameter in our optimization. We employ the BFGS algorithm as the classical optimizer, a quasi-Newton method for solving unconstrained nonlinear optimization problems. It achieves gradient descent by preconditioning the gradient without explicitly requiring the Hessian matrix.

In Fig. 2(a), we solve the MAX-CUT problem for a 2-regular graph using 50 different randomized initial parameters in each set, with $n = 3$ and 6 tunable parameters in the control pulses (25). To illustrate the dispersion and skewness of the data, we depict the distribution using box plots. We observe that extending the pulse length does not improve model performance; specifically, $T = 1$ is sufficient for the problem, although the performance is not entirely satisfactory. The BFGS algorithm often converges at a local minimum, hindering optimal model performance and preventing the attainment of the optimal solution of

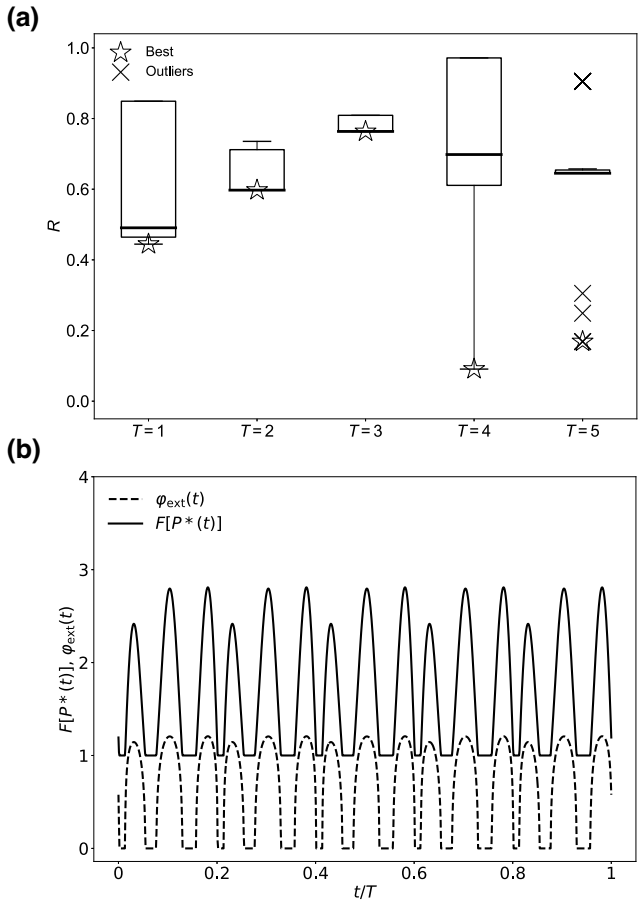

FIG. 2. (a) Error rate $R = |(\langle\Psi_f^*|\tilde{H}_p|\Psi_f^*\rangle - E_g)/E_g|$ of PBVQO for 2-regular graph MAX-CUT problem with 8 qubits. The boxplot represents the interquartile range (IQR) of the data, with the box spanning from the first quartile to the third quartile, and a line indicating the median. Whiskers extend from the box to the farthest data points within 1.5 times the IQR. Any data point beyond the whiskers is considered an outlier, denoted by a cross in the figure. Each best model performance over 50 random initializations of different operation times T is denoted by a star. (b) Optimal variational pulses $F[P^*(t)]$ and corresponding external flux $\varphi_{\text{ext}}(t)$ at $T = 5$. It results in the best error rate of $R = 0.168$. Optimal parameters: $\{A_1^* = 2.017,\ A_2^* = 0.644,\ A_3^* = 1.384,\ \phi_1^* = -0.141,\ \phi_2^* = -0.596,\ \phi_3^* = -0.408\}$. Dimensionless parameters for simulation of quantum dynamics: $\omega_1 = \omega_2 = \cdots = \omega_8 = 6$ and $G = 1$.

MAX-CUT after obtaining the classical string via measurement on the x-axis. In Fig. 2(b), we plot the control pulse and corresponding external flux for the best performance among all the initializations, which achieves an error rate of $R = 0.168$.

B. Metalearning

As we can see, the performance of variational algorithms heavily relies on parameter initialization. Adequate initialization can bring parameters close to the global minima, significantly reducing the iteration number. In the case of QAOA, one can utilize $\beta_i = B(i\delta t)\delta t$ and $\gamma_i = \Gamma(i\delta t)\delta t$ as digitized annealing schedules for $B(t)$ and $\Gamma(t)$, for instance, $B(t) = 1 - t/T$ and $\Gamma(t) = t/T$, instead of random initial parameters. However, the tunable pulse $P(t)$ does not conform to the standard quantum annealing paradigm since it is periodic, and the mixer is never turned off. In other words, there is no established initialization strategy for PBVQO. We propose a hypothesis that the optimal parameters $\{A_i^*, \phi_i^*\}$ found for minimizing an easier problem with an outstanding optimizer can serve as priors for a harder problem with a mediocre optimizer. This realization of metalearning for the harder problem as parameter initialization, even if the optimal parameters are not sufficiently close to the global minima, is our proposition.

C. Genetic optimization

To verify our hypothesis, we identify the easiest problem as a two-qubit MAX-CUT, which can be directly embedded in the minimal structure of our circuit (10). As observed, BFGS is highly sensitive to parameter initialization, making it suboptimal for our problem. Conversely, the genetic algorithm has been utilized to optimize quantum circuits and algorithms, demonstrating its ability for global search at the expense of considerable computational resources. While employing the genetic algorithm for optimizing the harder problem may be too complex, it is deemed acceptable for solving the two-qubit case and deriving parameters with maximal fitness.

In Fig. 3(a), we present the optimal control pulse $F[P^*(t)]$ for the two-qubit problem, achieving errorless ground state preparation. The corresponding parameters $\{A_i^*, \phi_i^*\}$ are then employed to initialize the BFGS optimizer for the 8-qubit problem, resulting in an initial error rate of $R = 0.744$. This initialization leads to $F[\tilde{P}^*(t)]$ [see Fig. 3(b)] that converges to $R = 0.056$, which is remarkably close to the exact ground state.

Furthermore, we establish the statistical significance of metalearning with the genetic algorithm over BFGS, demonstrating that the example in Fig. 3 is not cherry-picked. In Fig. 4, we depict the distribution of error rates R for the baseline (BFGS for 8-qubit), metalearning with BFGS, and metalearning with the genetic algorithm via histograms. In metalearning, we solve a two-qubit problem with the local optimizer BFGS and global optimizer GA, respectively, finding the exact solution $\langle\Psi_f|H_p|\Psi_f\rangle = -1$. Although both optimizers achieve good results on simpler problems, using two sets of optimal parameters as initialization for the local optimizer BFGS to solve the more challenging 8-qubit problem leads to different model performances. Therefore, we observe that metalearning with the genetic algorithm outperforms the other two

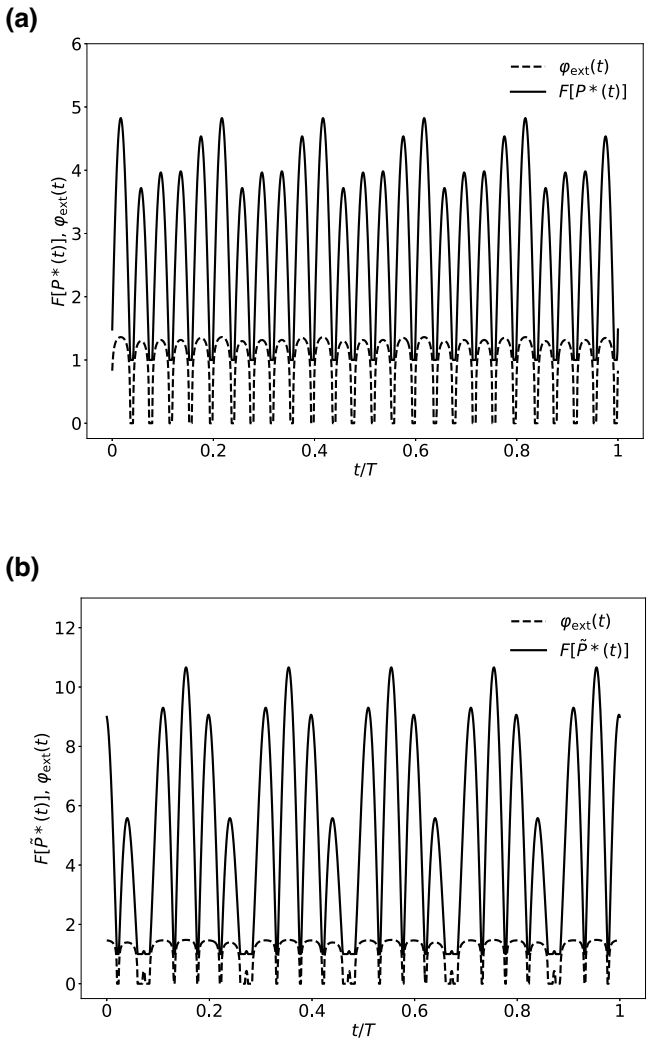

FIG. 3. (a) Optimal variational pulses $F[P^*(t)]$ and corresponding external flux $\varphi_{\text{ext}}(t)$ found by genetic algorithm for 2-qubit problem. Optimal parameters: $\{A_1^* = 0.307,\ A_2^* = 0.491,\ A_3^* = 4.202,\ \phi_1^* = 3.798,\ \phi_2^* = 3.253,\ \phi_3^* = 3.441\}$. (b) Optimal variational pulses $F[\tilde{P}^*(t)]$ and corresponding external flux $\varphi_{\text{ext}}(t)$ optimized by BFGS for 8-qubit problem, which is initialized by $\{A_i^*, \phi_i^*\}$ for 2-qubit problem with maximal fitness. Optimal parameters: $\{\tilde{A}_1^* = -1.668,\ \tilde{A}_2^* = 4.560,\ \tilde{A}_3^* = 6.861,\ \tilde{\phi}_1^* = 3.456,\ \tilde{\phi}_2^* = 3.919,\ \tilde{\phi}_3^* = 5.113\}$. Dimensionless parameters for simulation of quantum dynamics are the same as those before.

approaches. This finding supports the notion that employing a global optimizer to optimize an easy problem and using the result as parameter initialization for a harder problem is effective. In contrast, utilizing a local optimizer for an easier problem (see Meta-BFGS) does not overcome the local minimum in the harder one, even if it also solves the easier problem well. By showcasing the superiority of metalearning with the genetic algorithm, we provide the evidence supporting the efficacy of our approach in enhancing the performance of PBVQO.

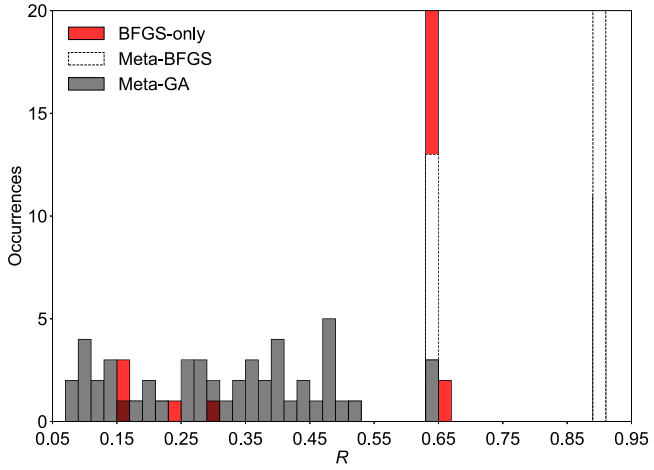

FIG. 4. Histogram of BFGS (baseline), metalearning with BFGS, and metalearning with genetic algorithm (GA) for 8-qubit QAOA.

V. DISCUSSION

After presenting the results of the numerical experiments with PBVQO, we proceed to compare them with conventional QAOA. As discussed in Sec. III, our digital-analog superconducting architecture facilitates direct implementation of XX rotation using gate Hamiltonian, avoiding the need for CNOT gates and local rotations. To establish a fair comparison, we initially assess the error rate of QAOA. Given that the performance of QAOA heavily depends on the depth p (equivalent to optimizing $2p$ variables), we set $p = 3$ for conventional QAOA, aligning with the 6 parameters in the pulse ansatz of PBVQO. Testing with 50 sets of random initial parameters, all of them converge to $R = 0.25$ for the 8-qubit MAX-CUT problem.

Another critical aspect is runtime, as longer runtimes accumulate errors due to quantum noise, particularly impactful in superconducting circuits. QAOA's runtime is directly related to single- and two-qubit gate times, implemented by corresponding gate Hamiltonians. The scale of Hamiltonians dictates gate times by requiring more energetic input within a shorter operation time. Along this, we calculate the energetic cost as [40]

$$C = \frac{1}{T}\int_0^T \|H(t)\|\, dt, \tag{26}$$

where $\|H(t)\|$ represents the Frobenius norm of the total Hamiltonian of PBVQO and the quantum gates in QAOA. A higher energetic cost indicates a longer runtime or, alternatively, a more intense pulse if the operation time is bounded. After averaging 50 independent simulations, we find $C_{\text{QAOA}} = 488.76$ for QAOA, while PBVQO incurs almost half the cost at $C_{\text{PBVQO}} = 280.87$.

While demonstrating the capability of our superconducting architecture in solving quantum optimization problems with PBVQO, surpassing conventional QAOA, it is essential to note that it is far from the optimal architecture for MAX-CUT problems. For instance, the regular QAOA embedding requires all-to-all connectivity, thus to be implemented in our platform it needs to perform swapping operations that add more complexity from the point of view of compilation and pulse levels because now the pulses ansatz requires learning such information. Alternatives approaches will include flux-qubit or transmon systems coupled to tunable couplers [41,42].

It is important to note that this pulse-based variational approach is not limited to superconducting circuits or circuit quantum electrodynamics architecture. The flexibility of our approach only requires a quantum platform capable of implementing time-dependent couplings and single-qubit rotations. Promising candidates should be Rydberg atoms [43–45] where one- or two-dimensional arrays of heavy alkali atoms such as rubidium (Rb) and cesium (Cs) are confined in optical tweezers, and single-qubit gates can be implemented by either microwave drives [46], optical stimulated Raman transitions, or a combination of microwave drives with magnetic field gradients [43] achieving gate fidelity for single-qubit rotations of $\mathcal{F} = 99.792\%$ [47]. Likewise, two-qubit interactions in Rb atoms have been implemented using the blockade effect with individual and separate addressing [43] and also with local spin exchange with atoms in movable tweezers [48].

Similarly, trapped ions [49,50] are viable for implementing our QAOA protocol. In this case, the microwave-controlled single-qubit operations are performed in the hyperfine energy levels, while the optical ones are made using stimulated Raman transitions for inducing quadrupolar transitions on the $D \rightarrow S$ levels [49], these approaches have achieved single-qubit fidelities around $\mathcal{F} = 99.993\%$ [51] for microwave and $\mathcal{F} = 99.995\%$ [52] for optical induced gates. Furthermore, there exist a plethora of ways for implementing two-qubit interaction in the platform; from Coulomb interaction [49], using coherently the motional degree of freedom of the quantized motion [53], and using such degree of freedom as a mediator for implementing a multiple-qubit interaction [54]. Theses approaches have achieved gate fidelities of $\mathcal{F} = 99.91\%$ [55] for hyperfine Mølmer-Sørensen gates.

VI. CONCLUSION AND OUTLOOK

In summary, we have introduced PBVQO as an extension to VQAs in the NISQ era. Our protocol is directly applicable to the superconducting circuit architecture within the digital-analog quantum computing paradigm. Through experiments solving the MAX-CUT problem, we have demonstrated PBVQO's capability to approximate the ground state of the problem Hamiltonian. Furthermore, we have proposed metalearning for parameter initialization in more challenging problems, utilizing a genetic algorithm as the global optimizer. The positive outcomes of metalearning with the global optimizer have been illustrated through benchmarking against baseline PBVQO and metalearning with a local optimizer. In addition, we have conducted comparisons with conventional gate-based QAOA and analyzed the mechanisms underlying its advantages.

Overall, the outlook for PBVQO is promising, with numerous open questions and opportunities for future research and development. For instance, investigating new optimization algorithms or adapting existing classical optimization methods to better suit the requirements of pulse-level optimization could lead to further improvements in performance and convergence speed. By extending pulse-based approaches to other prominent variational algorithms, such as VQE, one can potentially unlock new capabilities and address a wider range of optimization problems. Finally, as PBVQO continues to evolve, rigorous experimental validation and benchmarking against classical and quantum algorithms are essential. Thus, future study can be dedicated to the comprehensive experimental studies for validating the scalability, robustness, and performance of pulse-based techniques on noisy quantum hardware platforms, with error mitigation [56].

ACKNOWLEDGMENTS

This work is supported by NSFC (12075145 and 12211540002), STCSM (2019SHZDZX01-ZX04), and the Innovation Program for Quantum Science and Technology (2021ZD0302302), HORIZON-CL4-2022-QUANTUM-01-SGA project 101113946 OpenSuperQPlus100 of the EU Flagship on Quantum Technologies, the Basque Government through Grant No. IT1470-22. F.A.C.L. thanks the German Ministry for Education and Research, under QSolid, Grant no. 13N16149. This project has also received funding from the European Union's HORIZON Europe program via project HORIZON-CL4-2021-DIGITALEMERGING-02-10 (No. 101080085 QCFD).

[1] J. Preskill, Quantum computing in the NISQ era and beyond, Quantum **2**, 79 (2018).

[2] N. Moll, P. Barkoutsos, L. V. Bishop, J. M. Chow, A. Cross, D. J. Egger, S. Filipp, A. Fuhrer, J. M. Gambetta, and M. Ganzhorn, Quantum optimization using variational algorithms on near-term quantum devices, Quantum Sci. Technol. **3**, 030503 (2018).

[3] A. B. Finnila, M. A. Gomez, C. Sebenik, C. Stenson, and J. D. Doll, Quantum annealing: A new method for minimizing multidimensional functions, Chem. Phys. Lett. **219**, 343 (1994).

[4] P. Hauke, H. G. Katzgraber, W. Lechner, H. Nishimori, and W. D. Oliver, Perspectives of quantum annealing: Methods and implementations, Rep. Prog. Phys. **83**, 054401 (2020).

[5] E. J. Crosson and D. A. Lidar, Prospects for quantum enhancement with diabatic quantum annealing, Nat. Rev. Phys. **3**, 466 (2021).

[6] E. Farhi, J. Goldstone, and S. Gutmann, A quantum approximate optimization algorithm, arXiv:1411.4028.

[7] L. Zhou, S.-T. Wang, S. Choi, H. Pichler, and M. Lukin, Quantum approximate optimization algorithm: Performance, mechanism, and implementation on near-term devices, Phys. Rev. X **10**, 021067 (2020).

[8] M. Cerezo, A. Arrasmith, R. Babbush, S. C. Benjamin, S. Endo, K. Fujii, J. R. McClean, K. Mitarai, X. Yuan, L. Cincio, and P. J. Coles, Variational quantum algorithms, Nat. Rev. Phys. **3**, 625 (2021).

[9] K. Bharti, A. Cervera-Lierta, T.-H. Kyaw, T. Haug, S. Alperin-Lea, A. Anand, M. Degroote, H. Heimonen, J. S. Kottmann, T. Menke, W.-K. Mok, S. Sim, L.-C. Kwek, and Alán Aspuru-Guzik, Noisy intermediate-scale quantum algorithms, Rev. Mod. Phys. **94**, 015004 (2022).

[10] P. Vikstål, M. Grönkvist, M. Svensson, M. Andersson, G. Johansson, and G. Ferrini, Applying the quantum approximate optimization algorithm to the tail-assignment problem, Phys. Rev. Appl. **14**, 034009 (2020).

[11] P. Chandarana, N. N. Hegade, I. Montalban, E. Solano, and X. Chen, Digitized counterdiabatic quantum algorithm for protein folding, Phys. Rev. Appl. **20**, 014024 (2023).

[12] S. Brandhofer, D. Braun, V. Dehn, G. Hellstern, M. Hüls, Y. Ji, I. Polian, A. S. Bhatia, and T. Wellens, Benchmarking the performance of portfolio optimization with QAOA, Quantum Inf. Process. **22**, 25 (2023).

[13] Q.-M. Ding, Y.-M. Huang, and X. Yuan, Molecular docking via quantum approximate optimization algorithm, Phys. Rev. Appl. **21**, 034036 (2024).

[14] Z.-C. Yang, A. Rahmani, A. Shabani, H. Neven, and C. Chamon, Optimizing variational quantum algorithms using Pontryagin's minimum principle, Phys. Rev. X **7**, 021027 (2017).

[15] L. T. Brady, C. L. Baldwin, A. Bapat, Y. Kharkov, and A. V. Gorshkov, Optimal protocols in quantum annealing and quantum approximate optimization algorithm problems, Phys. Rev. Lett. **126**, 070505 (2021).

[16] A. Parra-Rodriguez, P. Lougovski, L. Lamata, E. Solano, and M. Sanz, Digital-analog quantum computation, Phys. Rev. A **101**, 022305 (2020).

[17] D. Headley, T. Müller, A. Martin, E. Solano, M. Sanz, and F. K. Wilhelm, Approximating the quantum approximate optimization algorithm with digital-analog interactions, Phys. Rev. A **106**, 042446 (2022).

[18] J. Biamonte, P. Wittek, N. Pancotti, P. Rebentrost, N. Wiebe, and S. Lloyd, Quantum machine learning, Nature **549**, 195 (2017).

[19] S. Hadfield, Z. Wang, B. O'Gorman, E. G. Rieffel, D. Venturelli, and R. Biswas, From the quantum approximate optimization algorithm to a quantum alternating operator ansatz, Algorithm **12**, 34 (2019).

[20] L. Zhu, H. L. Tang, G. S. Barron, F. A. Calderon-Vargas, N. J. Mayhall, E. Barnes, and S. E. Economou, Adaptive quantum approximate optimization algorithm for solving combinatorial problems on a quantum computer, Phys. Rev. Res. **4**, 033029 (2022).

[21] N. N. Hegade, K. Paul, Y. Ding, M. Sanz, F. Albarrán-Arriagada, E. Solano, and X. Chen, Shortcuts to adiabaticity in digitized adiabatic quantum computing, Phys. Rev. Appl. **15**, 024038 (2021).

[22] D. Sun, P. Chandarana, Z.-H. Xin, and X. Chen, Optimizing counterdiabaticity by variational quantum circuits, Phil. Trans. R. Soc. A **380**, 20210282 (2022).

[23] P. Chandarana, N. N. Hegade, K. Paul, F. Albarrán-Arriagada, E. Solano, A. del Campo, and X. Chen, Digitized-counterdiabatic quantum approximate optimization algorithm, Phys. Rev. Res. **4**, 013141 (2022).

[24] N. N. Hegade, X. Chen, and E. Solano, Digitized counterdiabatic quantum optimization, Phys. Rev. Res. **4**, L042030 (2022).

[25] R. Xu, J. Tang, P. Chandarana, K. Paul, X. Xu, M. Yung, and X. Chen, Benchmarking hybrid digitized-counterdiabatic quantum optimization, Phys. Rev. Res. **6**, 013147 (2024).

[26] O. R. Meitei, B. T. Gard, G. S. Barron, D. P. Pappas, S. E. Economou, E. Barnes, and N. J. Mayhall, Gate-free state preparation for fast variational quantum eigensolver simulations, npj Quantum Inf. **7**, 155 (2021).

[27] D. J. Egger, C. Capecci, B. Pokharel, P. K. Barkoutsos, L. E. Fischer, L. Guidoni, and I. Tavernelli, Pulse variational quantum eigensolver on cross-resonance-based hardware, Phys. Rev. Res. **5**, 033159 (2023).

[28] D. Meirom and S. H. Frankel, PANSATZ: Pulse-based ansatz for variational quantum algorithms, Front. Quantum Sci. Technol. **2**, 1273581 (2023).

[29] H.-X. Tao, J. He, and R.-B. Wu, Unleashing the expressive power of pulse-based quantum neural networks, arXiv:2402.02880.

[30] N. Barraza, G. Alvarado-Barrios, J. Peng, L. Lamata, E. Solano, and F. Albarrán-Arriagada, Analog quantum approximate optimization algorithm, Quantum Sci. Technol. **7**, 045035 (2022).

[31] N. Barraza, G. Alvarado-Barrios, I. Montalban, E. Solano, and F. Albarrán-Arriagada, Variational coherent quantum annealing, arXiv:2310.02248 [quant-ph].

[32] Y. Ji, K. F. Koenig, and I. Polian, Optimizing quantum algorithms on bipotent architectures, Phys. Rev. A **108**, 022610 (2023).

[33] P. Chandarana, P. Suárez-Vieites, N. N. Hegade, E. Solano, Y. Ban, and X. Chen, Meta-learning digitized-counterdiabatic quantum optimization, Quantum Sci. Technol. **8**, 045007 (2023).

[34] C. M. Unsal and L. T. Braddy, Quantum adversarial learning in emulation of Monte-Carlo methods for MAX-CUT approximation: QAOA is not optimal, arXiv:2211.13767 [quant-ph].

[35] J. Yu, J. C. Retamal, M. Sanz, E. Solano, and F. Albarrán-Arriagada, Superconducting circuit architecture for digital-analog quantum computing, EPJ Quantum Technol. **9**, 9 (2022).

[36] R. Johansson, G. Johansson, C. M. Wilson, and F. Nori, Dynamical Casimir effect in superconducting microwave circuits, Phys. Rev. A **82**, 052509 (2010).

[37] C. M. Wilson, G. Johansson, A. Pourkabirian, M. Simoen, J. R. Johansson, T. Duty, F. Nori, and P. Delsing, Observation of the dynamical Casimir effect in a superconducting circuit, Nature **479**, 376 (2011).

[38] Sergey Bravyi and David P. DiVincenzo and Daniel Loss, Schrieffer-Wolff transformation for quantum many-body systems, Ann. Phys. **326**, 2793 (2011).

[39] A. Deshpande, A. V. Gorshkov, and B. Fefferman, Importance of the spectral gap in estimating ground-state energies, PRX Quantum **3**, 040327 (2022).

[40] Obinna Abah, Ricardo Puebla, Anthony Kiely, Gabriele De Chiara, Mauro Paternostro, and Steve Campbell, Energetic cost of quantum control protocols, New J. Phys. **21**, 103048 (2019).

[41] Y. Sung, L. Ding, J. Braumüller, A. Vepsäläinen, B. Kannan, M. Kjaergaard, A. Greene, G. O. Samach, C. McNally, D. Kim, A. Melville, B. M. Niedzielski, M. E. Schwartz, J. L. Yoder, T. P. Orlando, S. Gustavsson, and W. D. Oliver, Realization of high-fidelity CZ and *ZZ*-free iSWAP gates with a tunable coupler, Phys. Rev. X **11**, 021058 (2021).

[42] L. Heunisch, C. Eichler, and M. J. Hartmann, Tunable coupler to fully decouple and maximally localize superconducting qubits, Phys. Rev. Appl. **20**, 064037 (2023).

[43] M. Saffman, Quantum computing with atomic qubits and Rydberg interactions: Progress and challenges, J. Phys. B: At. Mol. Opt. Phys. **49**, 202001 (2016).

[44] H. Levine, A. Keesling, G. Semeghini, A. Omran, T. T. Wang, S. Ebadi, H. Bernien, M. Greiner, V. Vuletić, H. Pichler, and M. D. Lukin, Parallel implementation of high-fidelity multiqubit gates with neutral atoms, Phys. Rev. Lett. **123**, 170503 (2019).

[45] A. Browaeys and T. Lahaye, Many-body physics with individually controlled Rydberg atoms, Nat. Phys. **16**, 132 (2020).

[46] I. Dotsenko, W. Alt, S. Kuhr, D. Schrader, M. Müller, Y. Miroshnychenko, V. Gomer, A. Rauschenbeutel, and D. Meschede, Application of electro-optically generated light fields for Raman spectroscopy of trapped cesium atoms, Appl. Phys. B **78**, 711 (2004).

[47] Y. Wang, A. Kumar, T.-Y. Wu, and D. S. Weiss, Single qubit gates based on targeted phase shifts in a 3D neutral atom array, Science **352**, 1562 (2016).

[48] A. M. Kaufman, B. J. Lester, M. Foss-Feig, M. L. Wall, A. M. Rey, and C. A. Regal, Entangling two transportable neutral atoms via local spin exchange, Nature **527**, 208 (2015).

[49] C. D. Bruzewicz, J. Chiaverini, R. McConnell, and J. M. Sage, Trapped-ion quantum computing: Progress and challenges featured, Appl. Phys. Rev. **6**, 021314 (2019).

[50] C. Monroe, W. C. Campbell, L.-M. Duan, Z.-X. Gong, A. V. Gorshkov, P. W. Hess, R. Islam, K. Kim, N. M. Linke, G. Pagano, P. Richerme, C. Senko, and N. Y. Yao, Programmable quantum simulations of spin systems with trapped ions, Rev. Mod. Phys. **93**, 025001 (2021).

[51] T. P. Harty, D. T. C. Allcock, C. J. Ballance, L. Guidoni, H. A. Janacek, N. M. Linke, D. N. Stacey, and D. M. Lucas, High-fidelity preparation, gates, memory, and readout of a trapped-ion quantum bit, Phys. Rev. Lett. **113**, 220501 (2014).

[52] A. Bermudez, X. Xu, R. Nigmatullin, J. O'Gorman, V. Negnevitsky, P. Schindler, T. Monz, U. G. Poschinger, C. Hempel, J. Home, F. Schmidt-Kaler, M. Biercuk, R. Blatt, S. Benjamin, and M. Müller, Assessing the progress of trapped-ion processors towards fault-tolerant quantum computation, Phys. Rev. X **7**, 041061 (2017).

[53] J. I. Cirac and P. Zoller, Quantum computations with cold trapped ions, Phys. Rev. Lett. **74**, 4091 (1995).

[54] A. Sørensen and K. Mølmer, Quantum computation with ions in thermal motion, Phys. Rev. Lett. **82**, 1971 (1999).

[55] J. P. Gaebler, T. R. Tan, Y. Lin, Y. Wan, R. Bowler, A. C. Keith, S. Glancy, K. Coakley, E. Knill, D. Leibfried, and D. J. Wineland, High-fidelity universal gate set for $^{9}Be^{+}$ ion qubits, Phys. Rev. Lett. **117**, 060505 (2016).

[56] Z. Cai, R. Babbush, S. C. Benjamin, S. Endo, W. J. Huggins, Y. Li, J. R. McClean, and T. E. O'Brien, Quantum error mitigation, Rev. Mod. Phys. **95**, 045005 (2023).